



TEMPERATURE SENSING ARRAY FOR PARALLEL MEASUREMENTS IN TUNNEL FIRE MODELS

Gallo M.¹, Kunsch J. P. and Rösgen T.

ABSTRACT

In order to optimize the emergency ventilation strategies put into operation during a tunnel fire, a better knowledge of the temperature field and the flow field generated by a tunnel fire is required. Tests have been conducted in a model tunnel at ETH for two different ventilation regimes indicating strong changes in the temperature field. An objective of the present work is to describe a new experimental technique allowing the measurement of both a two-dimensional temperature and velocity field. Preliminary experimental results showing the feasibility of this new technique are shown.

Keywords: Fire simulation, hot jet in confined cross-flow, temperature measurements, InfraRed Thermography.

INTRODUCTION

In the past years several catastrophic tunnel fires involving vehicles have occurred. Examples are the accidents in the Mont-Blanc tunnel (1999) and the Gotthard tunnel (2001). Although the number of tunnel kilometers is relatively small, an accident involving a fire in a tunnel has much more dramatic consequences than those which occur along the open roads. Indeed in case of fire, owing to the confined geometry of the tunnel, the temperature can easily exceed 1000 °C and the dispersion of smoke gases increases the asphyxia risk. Many studies have been conducted on this very complex phenomenon, since it involves combustion with chemical kinetics and fluid dynamics with complex turbulent structures. One important issue in fire safety is the longitudinal ventilation that should allow to control, in event of fire, the smoke dispersion. For this subject it is very important to introduce the concept of ‘critical ventilation velocity’, defined as the minimum air velocity required to suppress the smoke spreading against the longitudinal ventilation flow during tunnel fires. In experimental investigations on emergency ventilation systems, Vauquelin (2005) used a parametric approach to evaluate the critical velocity for different channel dimensions and for different buoyant sources. Wu and Bakar (2000) carried out experiments both to determine the critical velocity for different cross sectional geometries and to measure the temperature and the velocity in the tunnel. Lee and Ryou (2004) performed experiments to study the effects of the aspect ratio of a tunnel cross section on the critical velocity. Analytical models have been developed by Danziger and Kennedy (1982) and Kunsch (2002) to evaluate the critical velocity. In particular the latter

¹ Corresponding author: Institute of Fluid Dynamics, ETH Zurich, Sonneggstrasse 3, Zürich 8092, Switzerland, e-mail: gallo@ifd.mavt.ethz.ch

predicts the existence of an asymptotic value of the critical velocity for high heat release rates. The effect of the longitudinal ventilation on the burning rate in tunnel fires was studied by Yang et al. (2005) and by Roh et al. (2008) while Atkinson and Wu (1996) performed experiments for various tunnel slopes. Many numerical studies on tunnel fires are presented in the literature. Brandeis and Bergmann (1983) carried out two-dimensional simulations of fires in tunnels with forced ventilation under different ventilation regimes. Fletcher et al. (1994) studied the effects of the ventilation velocity and heat release rate of the fire. Ballesteros-Tajadura et al. (2006) put special emphasis on the study of the influence of the tunnel slope on the smoke behavior. The maximum smoke temperature under the ceiling of a tunnel was studied experimentally and numerically by Hu et al. (2006) while temperature and velocity data were acquired by Rusch et al. (2008) in order to have well defined boundary conditions for CFD simulations and experimental data for their validation. Recently a new simplified model for the simulation of fires in road tunnels with longitudinal ventilation has been proposed by Migoya et al. (2009).

Emergency ventilation strategies put into operation during a tunnel fire can be improved on the basis of a better understanding of the corresponding complex flow phenomena. The experimental facility at ETHZ was designed to attain this objective by physical modeling. Alternative tools, such as commercial software packages (e.g. CFX or FDS, especially designed for fires) provide a good insight in most of the fire scenarios, but their limitations become apparent in the prediction of entrainment and dilution involving turbulence modeling in a stratified environment. Hence an experimental investigation of the stratification related to the temperature field was performed. In addition, by means of 3D-reconstruction of the temperature field, a better understanding of the thermal behavior of the flow generated by a tunnel fire, consisting of the buoyancy driven flow in the fire plume interacting with active tunnel ventilation, should be attained. A further objective of the present work is to describe the basic physical principles which govern a new experimental technique that should allow a two-dimensional measurement of both the temperature and the main velocity. Preliminary experimental tests will be presented to demonstrate the feasibility of this new technique.

EXPERIMENTAL APPARATUS

The tunnel, sketched in Fig. 1, is mounted on a frame made of aluminum profiles. This design facilitates tilting of the complete tunnel to introduce streamwise buoyancy effects. The square cross section of the tunnel has a height of 0.8m. The air intake consists of a nozzle, with a contraction in only one direction and an area ratio of 1.75. Upstream of the nozzle three fabric screens and one screen made of stainless steel cause enough pressure loss to damp incoming disturbances from the laboratory. The ceiling and the side walls consist of insulating material, because the hot air propagates under the ceiling due to buoyancy. The floor is made of glass plates and allows optical access for LDA or PIV. The glass plates are 0.95m long, 6mm thick and are separated in the downstream direction by aluminum 5mm wide spaces which in turn can be replaced by a special plate containing ports for the thermocouple traversing rake. At the location of the hot air source the floor is made of a 0.95m long plate consisting of insulating material able to sustain the high temperatures. The hot air source is realized by an electric heater which allows to heat up the supplied air from the ambient temperature to about 500 °C. In order to smooth the velocity profiles downstream of the heater, two layers of fine stainless steel screen are inserted in the heater exit plane. A diffuser with an opening angle of 4 degrees is mounted downstream of the screens, followed by a pipe with an inner diameter of 0.2m. Both the diffuser and the pipe are insulated with two layers of 30mm thick stone wool mats. The extraction fan drives the cross-flow and is connected to the tunnel by a 0.5m long nozzle. This nozzle provides the transition of the square cross section to the circular one with a diameter of 0.6m. A 40mm thick honeycomb with a pitch of 5mm is mounted between the nozzle and the fan in order to prevent the formation of an upstream vortex generated by the fan. Three PID controllers are employed to assure the repeatability and stable operation of the experiments. The first

PID controller uses the analog signal of a velocity anemometer, located immediately after the tunnel inlet nozzle, to control the motor of the extraction fan. The second PID unit controls the blower which supplies the electric heater with air. It receives the input signal from a volumetric flow rate sensor and keeps the cold supply air volume constant. The third PID controller reads its signal from a K-type thermocouple which is placed downstream of the electric heater and maintains the jet temperature constant during the operation.

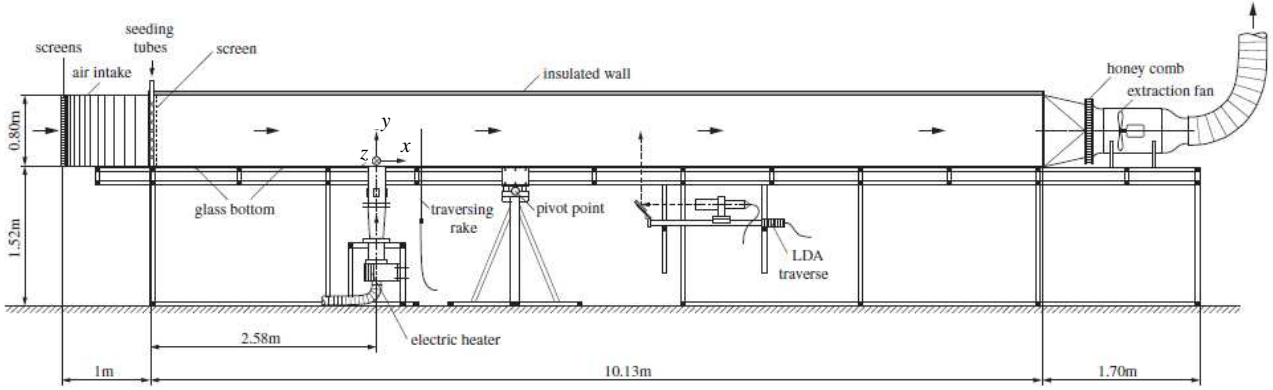


Fig. 1. Experimental set-up

TEMPERATURE MEASUREMENTS

In this section the applied measurement technique for the temperature is described and subsequently the experimental results will be discussed.

Experimental procedure

The dimensionless numbers which govern the thermo-fluid-dynamics behavior of the flow in the tunnel are the heat release rate \dot{Q}^* and the Richardson number Ri . The heat release rate is given by the following relations:

$$\dot{Q}^* = \frac{\dot{Q}}{\rho_{cf} C_p T_{cf} D^2 \sqrt{gD}} \quad (1)$$

$$\dot{Q} = \dot{m}_{hj} C_p (T_{hj} - T_a) \quad (2)$$

and the Richardson number is defined by the following ratio:

$$Ri = \frac{\Delta\rho g H}{\rho_a U_{cf}^2} \quad (3)$$

where ρ is the density, T the temperature, D the hot jet diameter, C_p the specific heat of the air, g the acceleration of gravity, $\Delta\rho$ the density rise above ambient, H the tunnel height, \dot{m} the mass flow rate and U the velocity. The subscript “a” refers to ambient condition, “cf” to the cross-flow and “hj” to the hot jet.

The choice of \dot{Q}^* , which characterizes the fire plume from the energetic point of view, is very important to simulate realistic fire conditions. Indeed, as discussed by Heskestad (2002), its value must be small enough to allow physical modeling of the buoyancy-driven pool fire regime. The cross-flow velocity, occurring in the Ri number which characterizes stratification, is an important parameter to be chosen carefully in the experiments. When the cross-flow velocity is too small, backlayering occurs, i.e. the hot-air plume can propagate upstream in opposite direction to the fresh air current. Backlayering may obstruct partially the cross section with the velocity anemometer used for the control of the extraction fan. This partial blockage would lead to an acceleration of the cold air flow and the velocity anemometer in the control loop would trigger a reduction of the cross flow velocity. As a consequence, enhanced backlayering would lead to global instability of the tunnel. However, when the cross-flow velocity is too large, entrainment of cold air into the hot jet would reduce the stratification below a relevant level.

The coordinate system adopted to localize the various investigated cross-sections downstream of the hot jet is shown in Fig. 1. The locations and the test conditions are also summarized in Tab. 1. The temperature measurements were conducted using NiCr-Ni Type-K thermocouples whose signals are acquired and amplified with a custom-built multichannel amplifier and are then logged with a A/D converter on a data acquisition board on a computer. In the generic tunnel cross section the temperature distributions are measured by means of rake which can contain up to 15 probes but, in order to avoid an excessive blockage, only eight or seven probes, respectively are traversed at the same time. The probes are equally spaced at 5cm in the span-wise direction and the step size in vertical direction is chosen to be 2.5cm. The first and the last port of the rake are both placed at a distance of 5cm from the two side walls. The measurement position of the thermocouples closest to the ceiling is 1.25cm. At each vertical station the temperatures are recorded with a sampling rate of $f_{sr}=50\text{Hz}$ over 3 minutes. In the different investigated tunnel cross sections, the mean temperature distributions are evaluated interpolating onto a square grid (31x31), the mean temperatures being measured on the 15x31 acquisition points. The mean temperature distributions, acquired in the various investigated sections of the tunnel, have been normalized by means of T_b defined by relation (4). The maps of the mean normalized temperature (T/T_b) have been used to perform a 3D-reconstruction of the temperature field in the test region of the tunnel which should provide a better insight into the fluid thermal behavior along the tunnel axis. In all the figures shown in the next subsection, the center of the circular exit section of the hot jet is located at $x/D=0$, $y/D=0.5$ and $z/D=0$ and the cross-flow direction corresponds to the x axis.

$$T_b = \frac{\dot{m}_{cf}T_{cf} + \dot{m}_{hj}T_{hj}}{\dot{m}_{cf} + \dot{m}_{hj}} \quad (4)$$

Table 1. Test conditions and investigated planes

Ri	\dot{Q}^*	Investigated sections		
		From	To	Pitch
4.75	0.95	$x/D=0.625$	$x/D=6.875$	$1.25D$
10.3	0.95	$x/D=0.625$	$x/D=6.875$	$1.25D$

Results

Fig. 2 reports, for the tunnel volume explored during the investigations, both the iso- T/T_b surfaces relative to the value of $T/T_b = 1.37$ and the slice $y/D=0.2$ for the two tested Richardson numbers. It is well known from the literature that the unbounded jet in cross-flow is characterized, downstream of the exit

section of the jet, by a counter-rotating vortex pair (CVP) with its axis along the cross-flow direction (Fric and Roshko (1994)). For both tested Richardson numbers, it is possible to observe for $T/T_b=1.37$ two separated iso- T/T_b surfaces which are associated with the CVP cited above.

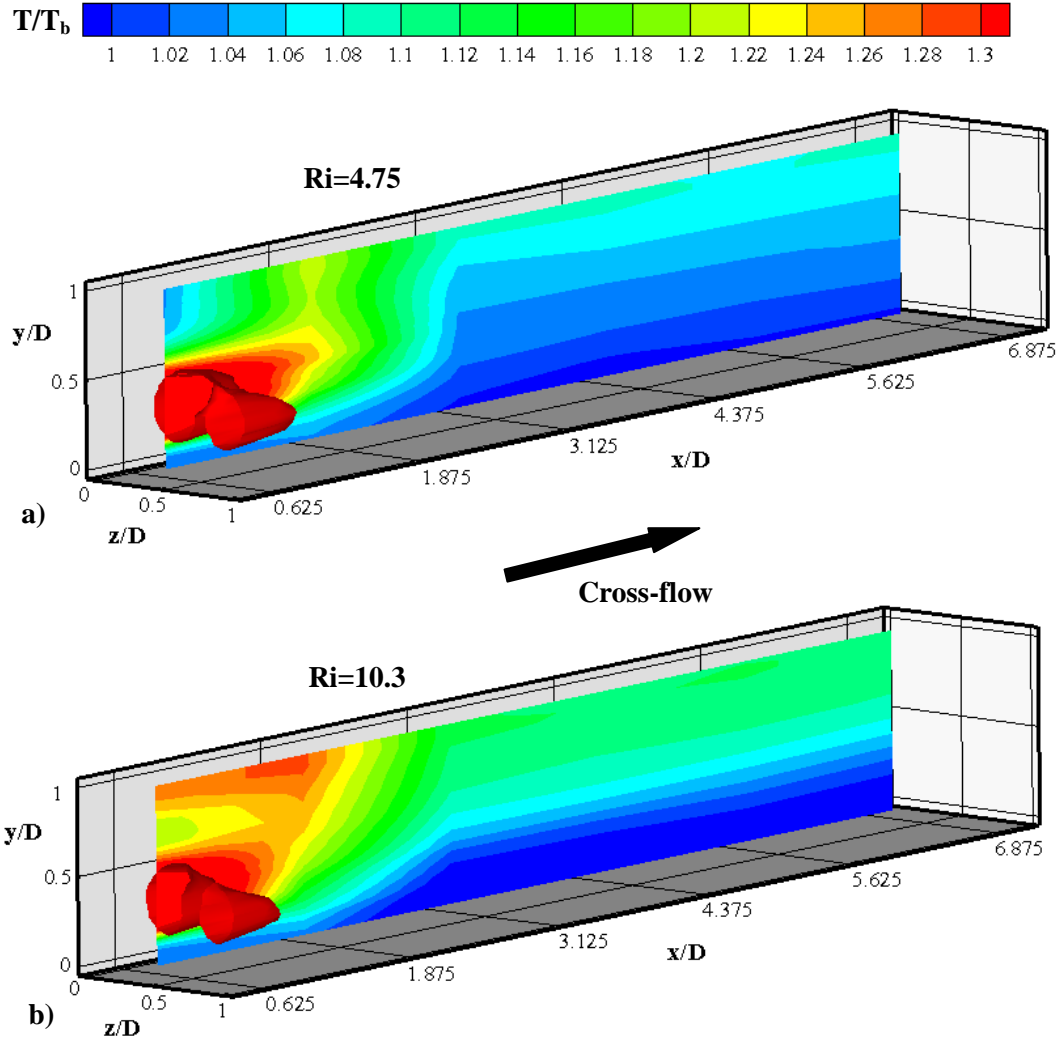


Fig. 2. Dimensionless temperature distribution at $y/D=0.2$ and iso- T/T_b surface for $T/T_b=1.37$: a) $Ri=4.75$; b) $Ri=10.3$.

For the lower Ri (Fig. 2a), i.e. for the higher cross-flow velocity, it can be noted that the cross-flow exhibits a better capability to wrap the CVP because the shear stresses on the boundaries between the two counter-rotating vortices and the cross-flow are more intense. The high kinetic energy contained in the cross-flow promotes a better cooling of the two hot counter-rotating vortices. In addition, the buoyancy effects of the hot jet become clearly visible. This is highlighted by the fact that, for $0.625 < x/D < 3.125$, in proximity of the ceiling the measured temperatures are lower than the ones measured, in the same region, for $Ri=10.3$ (Fig. 2b). When the cross-flow velocity is reduced, the buoyancy effects become stronger. Indeed, from the T/T_b distribution relative to $y/D=0.2$ and $Ri=10.3$ (Fig. 2b), it is possible to see in proximity of the ceiling ($0 < x/D < 1.875$) both a significant increase of the temperature and an upstream movement of the iso- T/T_b curves. This can be explained by a lower cross-flow rate and hence a higher

temperature of the two hot counter-rotating vortices reaching the ceiling and splitting in both directions, upstream and downstream. The upstream movement of the flow at the ceiling, known as backlayering, is absent in the case of $Ri=4.75$ (Fig. 2a). In fact at the inlet of the test region close to the ceiling, the measured temperatures appear to be very low. After the section $x/D=3.125$, Fig. 2 shows, for both the tested Richardson numbers, a stratification of the temperature, but the one with a stronger temperature gradient is that for $Ri=10.3$ (Fig. 2b).

From Fig. 3, reporting the iso- T/T_b surfaces for the value of $T/T_b=1.02$ for the two tested Richardson numbers, it is possible to see in case of a higher cross-flow velocity (Fig. 3a) that the iso- T/T_b surface shows a peak between $x/D=2$ and $x/D=4$, while the iso- T/T_b surface related to the lower cross-flow velocity (Fig. 3b) is rather flat. This different behavior could be explained by the fact that a high cross flow velocity produces a strong depression immediately after the hot jet that together with the rotation direction of the CVP should promote secondary flow fields responsible for the upwards movement of the cooler air close to the floor of the tunnel.

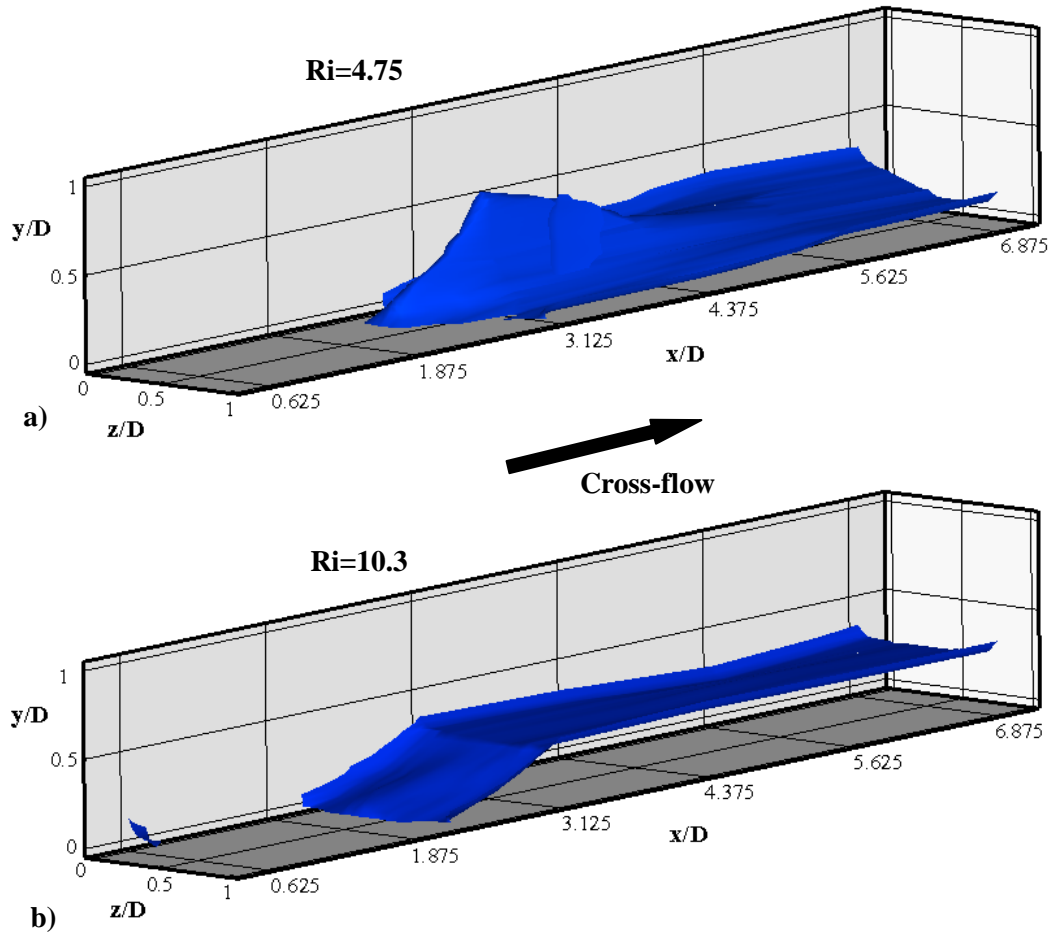


Fig. 3. Iso- T/T_b surface for $T/T_b=1.02$: a) $Ri=4.75$; b) $Ri=10.3$

HEATED GRID TECHNIQUE

Although thermocouple measurements are quite accurate, they are very time consuming, especially when a high spatial resolution is required. In order to overcome this drawback, a new experimental

technique is being developed. This technique allows to perform, in the tunnel cross-sections, a two-dimensional measurement of both the temperature and the main velocity. It requires the insertion into the flow field of a very high porosity grid (the sensor), normal to the main flow direction, which is formed by a thin electrically conductive wire having a high emissivity. The sensor surface temperatures are measured by means of an InfraRed (IR) camera.

Governing equations: fluid temperature measurements

The energy balance for an annular element of a long solid cylinder ($L \gg r$) with internal heat generation (Fig. 4) is provided by eq. 5. In this case the heat is generated as the result of the current passage in the wire of the sensor (Joule effect).

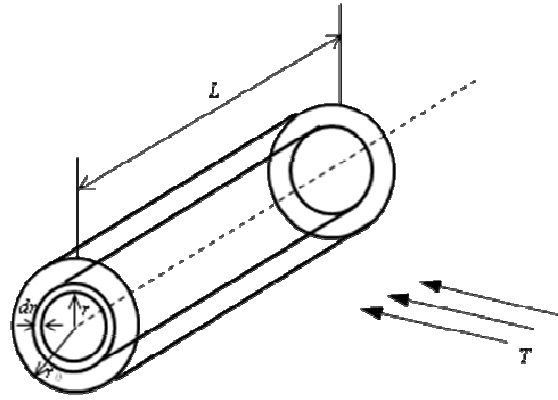


Fig. 4. Circular cylinder with internal heat generation

$$q_G r = -k \frac{d}{dr} \left(r \frac{dT}{dr} \right) \quad (5)$$

If the solid cylinder is immersed in a fluid at a temperature T_f the boundary conditions require that the heat conduction from the cylinder equals the rate of the convection and radiation at the surface:

$$-k \frac{dT}{dr} \Big|_{r=r_0} = \bar{h}_c (T_0 - T_f); \quad T(r = r_0) = T_0$$

where \bar{h}_c and T_0 are, respectively, the heat transfer coefficient and the temperature at the specified surface $r=r_0$. By using the boundary conditions above it is possible to obtain the temperature distribution in the wire cross section:

$$T(r) - T_f = \frac{q_G r_0}{4h_c} \left\{ 2 + \frac{\bar{h}_c r_0}{k} \left[1 - \left(\frac{r}{r_0} \right)^2 \right] \right\} \quad (6)$$

The ratio $\frac{\bar{h}_c r_0}{k}$ represents the Biot number (Bi) which provides the relative importance of the conductive thermal resistance $R_k = r_0/k$ and the convective resistance $R_c = 1/\bar{h}_c$. If the Biot number approaches

zero, the solid can be considered isothermal in the section normal to longitudinal axis of the wire and the temperature change is principally at the fluid-solid interface. If the material and the diameter of the wire forming the sensor are such as to assure, for the considered flow field, a Bi significantly smaller than one eq. 6 can be rewritten ².

$$\frac{q_G r_0}{2} = \bar{h}_c (T - T_f). \quad (7)$$

The heat transfer coefficient \bar{h}_c is the sum of the convective (h_c) and radiative (h_r) heat transfer coefficients:

$$\bar{h}_c = (h_c + h_r). \quad (8)$$

Substituting eq. 8 into eq. 7 and imposing $T = T_{mh}$ leads to

$$\frac{q_G r_0}{2} = h_c (T_{mh} - T_f) + h_r (T_{mh} - T_f) \quad (9)$$

with

$$h_r = \frac{\sigma \mathcal{E} (T_{mh}^4 - T_{amb}^4)}{(T_{mh} - T_f)}. \quad (10)$$

The temperature T_{amb} is the ambient temperature in case of not confined flows, while for the confined ones T_{amb} is the bulk temperature T_b (eq. 4). Taking into account the expression of h_r (eq. 10), eq. 9 becomes

$$\frac{q_G r_0}{2} = h_c (T_{mh} - T_f) + \sigma \mathcal{E} (T_{mh}^4 - T_{amb}^4). \quad (11)$$

In absence of heat generation ($q_G=0$) eq. 11, by imposing $T = T_{mc}$, can be written

$$0 = h_c (T_{mc} - T_f) + \sigma \mathcal{E} (T_{mc}^4 - T_{amb}^4). \quad (12)$$

Subtracting eq. 11 from 12 it is possible to evaluate the convective heat transfer coefficient h_c by the following equation:

$$h_c = \frac{1}{(T_{mh} - T_{mc})} \left[\frac{q_G r_0}{2} - \sigma \mathcal{E} (T_{mh}^4 - T_{mc}^4) \right] \quad (13)$$

The sensor temperature distributions obtained by the IR camera relative to the heated case ($q_G > 0$, $T = T_{mh}$) and to the un-heated case ($q_G = 0$, $T = T_{mc}$) allow to evaluate by means of eq. 13 the convective heat transfer coefficient distribution (h_c) that, substituted in the eq. 11 or 12, furnishes the fluid temperature distributions T_f .

² Eq. 7 can be equally obtained by performing an overall energy balance:

$$q_G (\pi r_0^2 L) = \bar{h}_c (2\pi r_0 L) (T - T_f)$$

Governing equations: fluid velocity measurements

The “*hot grid technique*” allows to evaluate both the local convective heat transfer coefficient h_c and the local fluid temperature T_f . From the knowledge of T_f and h_c it is possible to evaluate the local distribution of the Nusselt number Nu defined as

$$Nu = \frac{h_c d}{\lambda}, \quad (14)$$

where d is the diameter of the wire and λ is the thermal conductivity of air estimated at the film temperature T_{film} expressed by the following relation:

$$T_{film} = \frac{T_m + T_f}{2}. \quad (15)$$

The local distribution of the Nusselt number can be used to evaluate, by means of King’s law (eq.16), the corresponding local distribution of the Reynolds number Re yielding the local velocity V perpendicular to the wire.

$$Nu = a + b Re^m \quad (16)$$

with

$$Re = \frac{Vd}{\nu} \quad (17)$$

where the kinematic viscosity ν is evaluated at the film temperature (eq. 15). The constants a , b and m are determined by means of a calibration procedure. For sake of brevity this procedure is not described in the present work.

Experimental procedure for the temperature measurements

In this section the new experimental procedure used to measure the fluid temperature is described. As a preliminary test case it was decided to measure, using a single *Cu-Ni* wire of 0.5mm diameter, the fluid temperature profile of a free hot jet (Fig. 5). The distance between the circular exit section ($d=6\text{cm}$) of the hot source and the wire was 40cm. The single wire is heated up by using an electronic power supply. The wire temperatures, used to evaluate the fluid temperature, are measured using an InfraRed camera with a mid-range infrared FPA (Focal Plane Array) InSb sensor (3 – 5 μm) of 320x240 pixels. A 50mm lens is used during the test at a distance of about 1.3m. A first step of this procedure requires a calibration which is described in the next subsection.

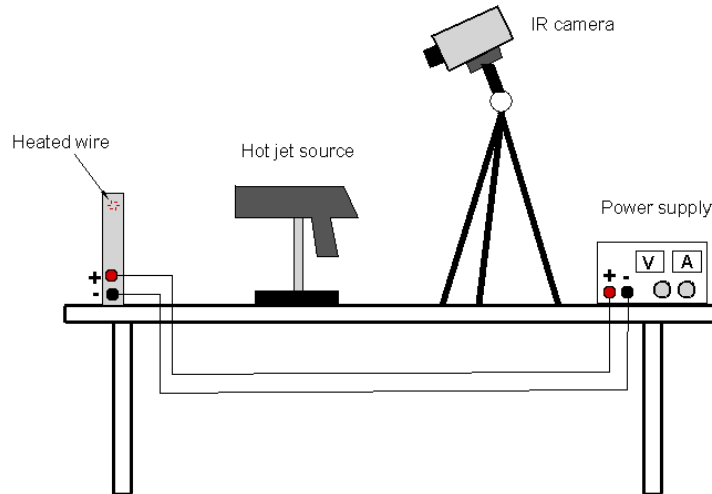


Fig. 5. Heated grid technique: layout of the preliminary test case

Calibration

The objective of the calibration is to acquire a family of curves which furnishes the Digital Level (DL) distribution along the wire for different heating levels, i.e. for different wire temperatures (Fig. 6). For a fixed heating level the wire temperature is measured by using a RTD and a screen is positioned immediately under the heated wire in order to limit the cooling effects associated with the natural convection. The DL distribution is obtained performing, for each column of the thermal image (Fig. 7a), the average of the maximum DL given by the pixel crossed by the heated wire and of the two DLs of the vertical neighbours (Fig. 7b). The distance between the wire and the IR camera is such that the wire diameter covers only partially the pixel surface. So, each pixel will provide a signal that is related to the mean temperature between the background and the wire temperature. For this reason, the background thermal image has been subtracted from each wire thermal image relative to the different heating levels, with the aim to isolate the pixel signal portion associated with the heated wire.

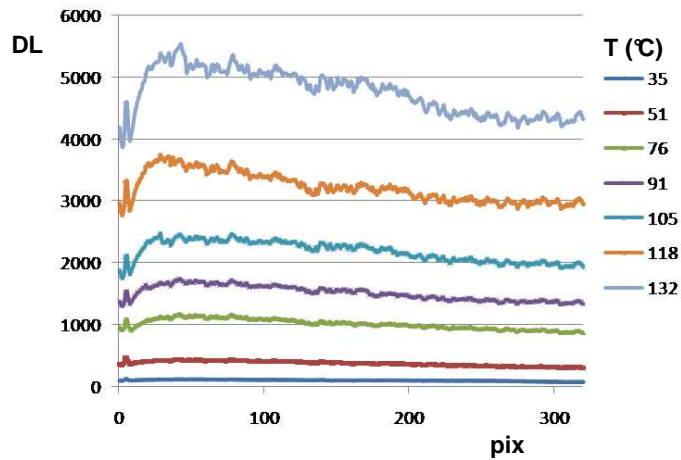


Fig. 6. Calibration curves

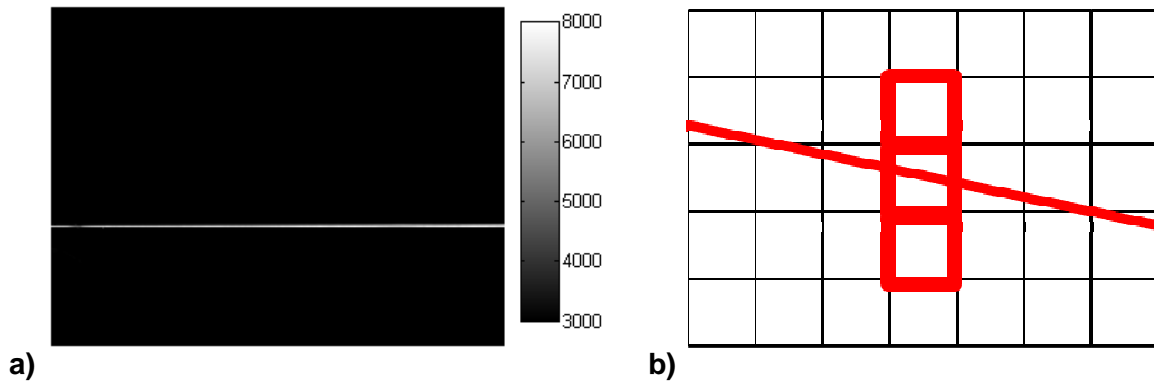


Fig. 7. Calibration: a) Thermal image of the wire; b) Scheme for the evaluation of the DL profile.

Fluid temperature measurements

To measure the fluid temperature profile it is necessary to acquire the DL distributions for two different heating levels of the wire immersed into the flow field (Fig. 8a). The DL profiles reported in Fig. 8a can be converted in temperatures by using the family of curves (Fig. 6) acquired during the calibration. The wire temperature profiles relative to the two heating levels were used to evaluate the convective heat transfer coefficient distributions h_c (eq. 13) and by using eq. 11 or 12 the fluid temperature profile (Fig. 8b).

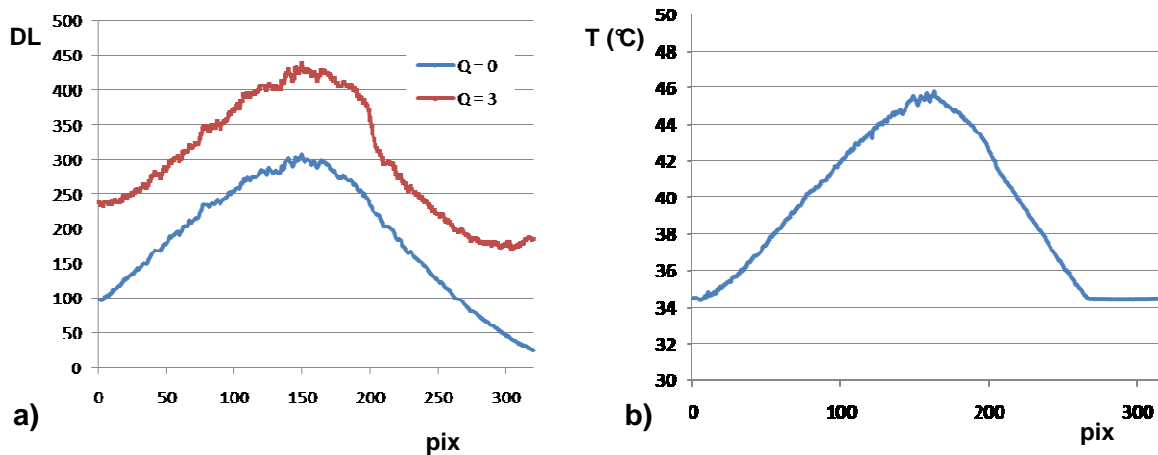


Fig. 8. Fluid temperature measurement: a) wire DL distributions for two different heating levels (Q=0W and Q=3W); b) Fluid temperature profile.

CONCLUSIONS

Measurements of the mean temperature field in different cross sections of a model tunnel in case of a fire have been carried out by using a rake of thermocouples. These measurements were used to perform a 3D reconstruction of the temperature field which allowed to highlight significant differences between the two tested ventilation regimes characterized by different temperature stratifications, as expressed by different Richardson numbers.

First experimental results related to a novel fluid temperature measurement with the “Heated Grid Technique” are promising. Further investigations are required both to define and to improve the accuracy of this new experimental technique, especially also regarding its potential for simultaneous temperature and velocity measurements.

REFERENCES

- Vauquelin O. (2005), “Parametrical study of the back flow occurrence in case of a buoyant release into a rectangular channel”, *Experimental Thermal and Fluid Science*, 29, 725-731.
- Wu Y. and M.Z.A. Bakar (2000), “Control of smoke flow in tunnel fires using longitudinal ventilation system – a study of critical velocity”, *Fire Safety Journal*, 25(4), 363-390.
- Lee S.R. and H.S. Ryou (2004), “An experimental study of the effect of the aspect ratio on the critical velocity in longitudinal ventilation tunnel fires”, *Journal of Fire Sciences*, 23, 119-138.
- Danziger N.H. and W.D. Kennedy (1982), “Longitudinal ventilation analysis for the Glenwood Canyon Tunnels”, 4th International Symposium on Aerodynamics and Ventilation of Vehicles Tunnels, BHR Group, 169-186
- Kunsch J.P. (2002), “Simple model for control of fire gases in a ventilated tunnel”, *Fire Safety Journal*, 37, 67-81.
- Yang S.S., S.C. Kim and H.S. Ryou (2005), “An experimental study on the effects of longitudinal ventilation on the variation of the burning rate in tunnel fires”, *Tunnel and Underground Space*, 15(1), 55-60.
- Roh J.S., S.S. Yang, H.S. Ryou, M.O Yoon and Y.T. Jeong (2008), “An experimental study on the effect of ventilation velocity on burning rate in tunnel fires – heptane pool fire case”, *Building and Environment*, 43, 1225-1231.
- Atkinson G.T. and Y. Wu (1996), “Smoke control in sloping tunnels”, *Fire Safety Journal*, 27, 335-341.
- Brandeis J. and D.J. Bergmann (1983), “A numerical study of tunnel fires”, *Combustion Science and Technology*, 35, 133-135.
- Fletcher D.F., J.H. Kent, J.H. Apte and A.R. Green (1994), “Numerical simulations of smoke movement from a pool fire in a ventilation tunnel”, *Fire Safety Journal*, 23, 305-325.
- Ballesteros-Tajadura R., C. Santolaria-Morros and E. Blanco-Marigorta (2006), “Influence of the slope in the ventilation semi-transversal system of an urban tunnel”, *Tunneling and Underground Space Technology*, 21, 21-28.
- Hu L.H., R. Huo, Y.Z. Li, W. Peng, W.K. Chow and R.X. Yang, “On the maximum smoke temperature under the ceiling in the tunnel fires”, *Tunneling and Underground Space Technology*, 21, 650-655.
- Rusch D., L. Blum, A. Moser, T. Roesgen (2008), “Turbulence model validation for fire simulation by CFD and experimental investigation of a hot jet in cross-flow”, *Fire Safety Journal*, 43, 429-441.
- Migoya E., A. Crespo, J. Garcia and J. Hernandez (2009), “A simplified model of fires in road tunnels. Comparison with three-dimensional models and full-scale measurements”, *Tunneling and Underground Space Technology*, 24, 37-52.
- Heskestad G. (2002), “Fire plumes, flame height and air entrainment”, *The SFPE Handbook of Fire Protection Engineering*, National Fire Protection Association, NY.
- Fric T.F. and A. Roshko (1994), “Vortical structure in the wake of a transverse jet”, *Journal of Fluid Mechanics*, 279, 1-47.